Endocrine Journal 2013, **60** (12), 1329-1334

ORIGINAL

Critical role of Yp inversion in *PRKX/PRKY*-mediated Xp;Yp translocation in a patient with 45,X testicular disorder of sex development

Shinichi Nakashima[1)], Yoriko Watanabe[2)], Junichiro Okada[2)], Hiroyuki Ono[1)], Eiko Nagata[1)], Maki Fukami[3)] and Tsutomu Ogata[1)]

[1)]*Department of Pediatrics, Hamamatsu University School of Medicine, Hamamatsu 431-3192, Japan*
[2)]*Department of Pediatrics, Kurume University School of Medicine, Kurume 830-0011, Japan*
[3)]*Department of Molecular Endocrinology, National Research Institute for Child Health and Development, Tokyo 157-8535, Japan*

Abstract. 45,X testicular disorder of sex development (TDSD), previously known as 45,X maleness, with unbalanced Xp;Yp translocation is an extremely rare condition caused by concomitant occurrence of loss of an X chromosome of maternal origin and an aberrant Xp;Yp translocation during paternal meiosis. We identified a Japanese male infant with an apparently 45,X karyotype who exhibited chondrodysplasia punctata and growth failure. Cytogenetic analysis revealed a 45,X.ish der(X)t(X;Y)(p22.33;p11.2)(DXZ1+,SRY+) karyotype. Array comparative genome hybridization analysis showed a simple Xp terminal deletion involving *SHOX* and *ARSE* with the breakpoint just centromeric to *PRKX*, and an apparently complex Yp translocation with the middle Yp breakpoint just telomeric to *PRKY* and the centromeric and the telomeric Yp breakpoints around the long inverted repeats for the generation of a common paracentric Yp inversion. Subsequently, a long PCR product was obtained with an X-specific and a Y-specific primers that were designed on the assumption of the presence of a Yp inversion that permits the alignment of *PRKX* and *PRKY* in the same direction, and the translocation fusion point was determined to reside within a 246 bp X-Y homologous segment at the "hot spot A" in the 5' region of *PRKX/PRKY*, by sequential direct sequencing for the long PCR product. These results argue not only for the presence of rare 45,X-TDSD with Xp;Yp translocation, but also for a critical role of a common paracentric Yp inversion in the occurrence of *PRKX/PRKY*-mediated unbalanced Xp;Yp translocation.

Key words: 45,X testicular DSD, Xp;Yp translocation, *PRKX/PRKY*, Yp inversion

45,X TESTICULAR DISORDER of sex development (TDSD) (previously known as 45,X maleness) with unbalanced Xp;Yp translocation is an extremely rare condition caused by concomitant occurrence of loss of an X chromosome of maternal origin and an aberrant Xp;Yp translocation during paternal meiosis [1, 2]. To our knowledge, this condition has been documented only in two patients [1, 2], although another 45,X-TDSD patient with apparent mosaicism for normal X chromosome and abnormal der(X)t(Xp;Yp) chromosome harboring *SRY* has also been documented [3].

For the unbalanced Xp;Yp translocation, previous studies in patients with *SRY*-positive 45,X-TDSD and 46,XX-TDSD (previously known as 46,XX maleness) and in those with *SRY*-negative 46,XY gonadal dysgenesis (previously known as 46,XY femaleness) have indicated the frequent occurrence of aberrant translocations between the homologous genes *PRKX* and *PRKY* [4-7]. In particular, most *PRKX/PRKY*-mediated translocations have taken place at two hot spots, *i.e.*, the "hot spot A" at the 5' sequence that shares 97% sequence similarity over 1.7 kb and even 98.7% sequence similarity over 1.2 kb and the "hot spot B" around the C-terminal coding region that shares 90% sequence similarity over 2 kb and even 96% sequence similarity over 1 kb [5]. In this regard, although such translocations are predicted to occur when *PRKX* and *PRKY* are aligned in the same direction, *PRKX* and *PRKY* are usually oriented in a reverse direction. However, *PRKX* and *PRKY* are aligned in the same direction in a subgroup of males with a common ~3.5 Mb paracentric Yp

Submitted Aug. 11, 2013; Accepted Sep. 6, 2013 as EJ13-0334
Released online in J-STAGE as advance publication Oct. 3, 2013
Correspondence to: Tsutomu Ogata, Department of Pediatrics, Hamamatsu University School of Medicine, 1-20-1 Handayama, Higashi-ku, Hamamatsu 431-3192, Japan.
E-mail: tomogata@hama-med.ac.jp

inversion probably caused by a homologous recombination between ~300 kb long inverted repeats [7, 8]. It has been suggested, therefore, that *PRKX/PRKY*-mediated translocations are prone to occur in Yp inversion positive males [7, 9].

Here, we report a 45,X-TDSD patient with Xp;Yp translocation. Cytogenetic and molecular studies in this patient argue not only for the presence of rare 45,X-TDSD with Xp;Yp translocation, but also for a critical role of a common paracentric Yp inversion in the occurrence of *PRKX/PRKY*-mediated unbalanced Xp;Yp translocation.

Case Report

Patient

This Japanese patient was referred to Kurume University Hospital at 28 weeks of gestation because of intrauterine growth retardation and mild short limbs that were identified by routine fetal ultrasound examinations. Subsequent pregnant course was uneventful, although he remained small for gestational age. The non-consanguineous parents were clinically normal.

He was born at 38 weeks of gestation after an uncomplicated vaginal delivery. His birth length was 40.2 cm (–3.4 SD), birth weight 2.29 kg (–2.2 SD), and birth occipitofrontal circumference (OFC) 28.8 cm (–3.0 SD). Physical examination revealed relatively short limbs and depressed nasal bridge. External genitalia were well masculinized. There were no discernible Turner syndrome soft tissue and visceral features, such as webbed neck, lymphedema, and cardiovascular and renal lesions. Radiological studies showed atlantoaxial subluxation and stippled calcifications at the bilateral proximal humeri, proximal femur, proximal tibias, and ankles, and neonatal audiometry tests revealed hearing loss (right 50 dB, left 80 dB). Thus, he was diagnosed as having X-linked recessive chondrodysplasia punctata (CDPX1). On the last examination at six months of age, he manifested severe growth failure, with a length of 55.7 cm (–5.0 SD), a weight of 5.20 kg (–3.1 SD), and an OFC of 41.0 cm (–1.8 SD).

Cytogenetic studies

G-banding analysis was performed at a 550-band resolution level, indicating a 45,add(X)(p22.33) karyotype in all the 50 lymphocytes examined. Fluorescence *in situ* hybridization analysis delineated positive signals for *DXZ1* and *SRY* on the same chromosome in all the 200 metaphases examined. Thus, his karyotype was determined as 45,X.ish der(X)t(X;Y)(p22.33;p11.2)(DXZ1+,SRY+). Parental karyotypes were apparently normal.

Array comparative genome hybridization analysis (CGH)

Oligonucleotide-based array CGH was performed for leukocyte genomic DNA, using (1) the Agilent G4447A Sure Print G3 Human CGH 1X1M Oligo Microarray kit containing 1 million catalog probes for the whole genome (Agilent Technologies, Santa Clara, CA, USA); and (2) a custom-build array containing 857,877 probes for the X-differential region and 54,388 probes for the Y-differential region, as well as ~10,000 reference probes for other chromosomal region. The procedure was as described in the manufacturer's instructions.

Array CGH showed a ~3,670,000 bp simple Xp terminal deletion involving *SHOX* and *ARSE*, with the breakpoint around the *PRKX* "hot spot A", and an apparently complex Yp translocation involving a ~6,120,000 bp terminal Yp region and a ~2,590,000 bp region between ~7,100,000 bp and ~9,690,000 bp from the Yp telomere, with the middle Yp breakpoint around the *PRKY* "hot spot A" (Fig. 1). Furthermore, the centromeric and the telomeric Yp breakpoints resided around the long inverted repeats for the common ~3.5 Mb paracentric Yp inversion [8]. These findings indicated that the paternal Y chromosome was accompanied by a paracentric Yp inversion, and that the *SRY*-positive X chromosome was generated by a simple Xp;Yp translocation at the *PRKX/PRKY* "hot spot A".

Determination of the translocation fusion point

To determine the translocation fusion point, we first performed PCR analysis using multiple primers for Xp-specific and Yp-specific loci around the breakpoints indicated by array CGH (Table 1). The Xp breakpoint was localized to a ~2,000 bp region between *XPBP3* and *XPBP4* (*XPBP1–XPBP4* were first designated in this study). While the results of Y-specific loci were apparently complex, they were interpreted as indicative of a single Yp breakpoint at a ~337,000 bp region between *PRKY* and *TBL1Y*, on the assumption of the presence of a paracentric Yp inversion (Fig. 2A).

Subsequently, long PCR was carried out using multiple primer sets for the localized Xp and Yp breakpoint segments, and a ~5.4 kb long PCR product was obtained with an Xp-specific primer and a Yp-specific primer (Table 2). Finally, direct sequencing was sequentially performed for the long PCR product, and the translocation fusion point

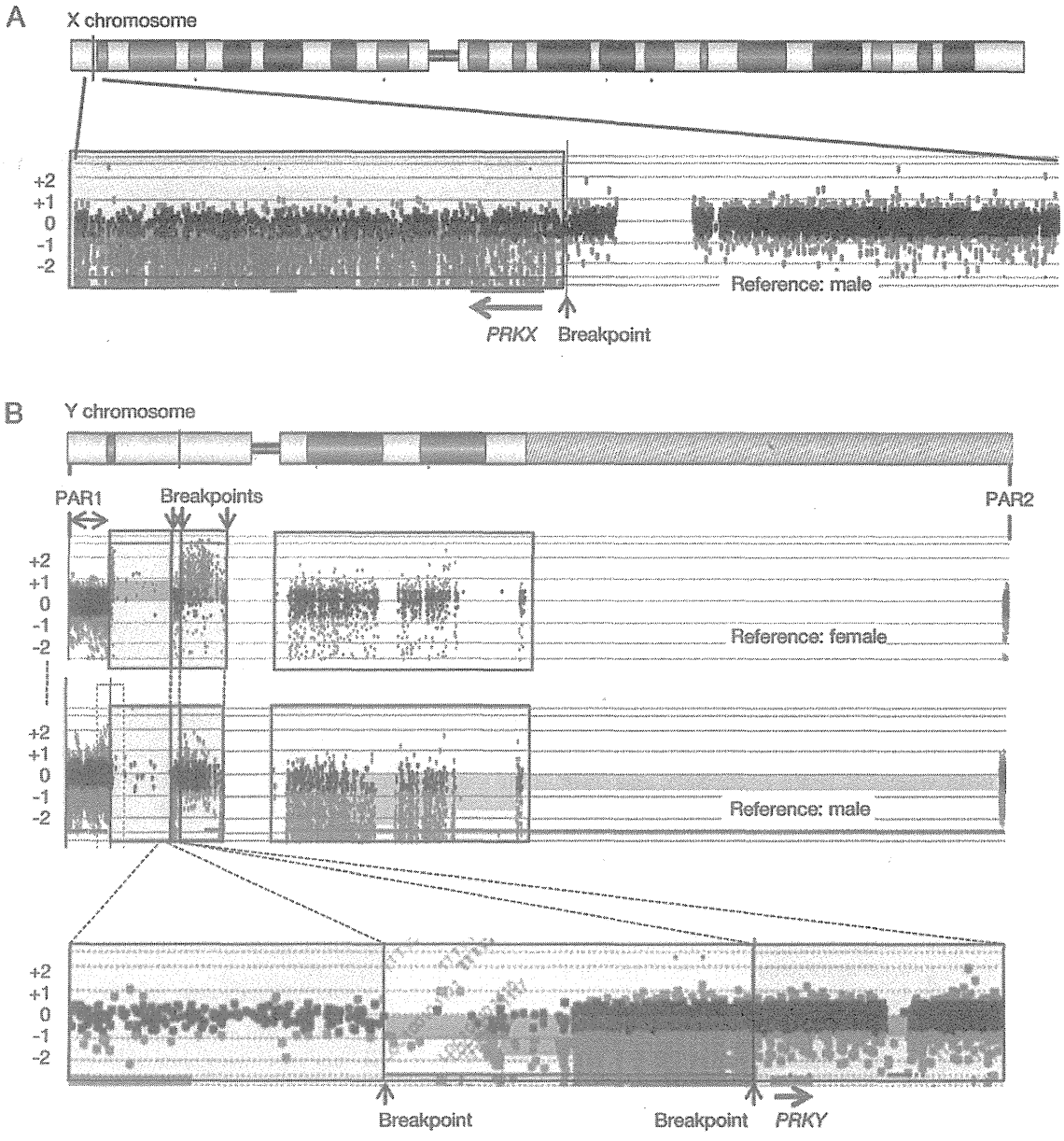

Fig. 1 Representative results of array CGH analysis. The black, the red, and the green dots denote signals indicative of the normal, the increased (> +0.5), and the decreased (< –1.0) copy numbers, respectively.

(A) A simple Xp terminal deletion with the breakpoint just centromeric to *PRKX*. An X-differential region encompassing the breakpoint is magnified. The red arrow indicates the transcriptional direction of *PRKX*. The data have been obtained with a custom-build high density probes for the X-differential region, using a genomic DNA sample from a normal male as a reference. The deleted region is highlighted with light blue.

(B) An apparently complex Yp translocation with the middle breakpoints just telomeric to *PRKY*. The blue arrow indicates the transcriptional direction of *PRKY*. The upper and the middle array findings have been obtained with 1 million catalog probes for the whole genome, using genomic DNA samples from a normal male and a normal female as references, and the lower array finding have been obtained with a custom-build high density probes for the Y-differential region, using a genomic DNA sample from a normal male as a reference. The data indicate the presence of two Y-differential regions (highlighted with light orange) and the absence of the remaining Y-differential region including a small region between the two positive Y-differential regions (highlighted with light yellow), as well as the single copies of the short arm and long arm pseudoautosomal regions (PAR1 and PAR2).

Table 1 Primers utilized in the localization of the translocation fusion point.

Locus (STS)	Forward	Reverse	Amplified segment[a]	AT	Results
X-specific locus					
XPBP1	GCTGTCTCCCATTCCTGAGA	GCCCTCACCAGACACTGAAT	3,663,463 ~ 3,663,700 bp	58	–
XPBP2	CCATGCACTCTTGCTGGTAA	CGTGCATTAAATGTGATCGTG	3,665,692 ~ 3,665,904 bp	58	–
XPBP3	GGGTGGTTAGTGTGACCCAG	ACAATGAGCTGCCTCCCAAA	3,671,443 ~ 3,671,599 bp	58	–
XPBP4	CCCTTCCCTCCCTTCCTTCT	GAATGGGCACGAAAATCATGCT	3,673,439 ~ 3,673,639 bp	58	+
Y-specific locus					
SHGC-79134	TATCTTTGTTTCTTGCAGCGTG	TGGAAGTGGGAGTGGAGATAAA	6,104,095 ~ 6,10,4376 bp	60	+
G65838 (sY605)	ACCTCCGAAGACTGAACCAG	CCCTTGAGTCCACAGAGTCC	6,616,473 ~ 6,61,6751 bp	58	–
AMELY (sY276)	CCTACCGCATCAGTGAATTTC	TCTGTATGTGGAGTACACATGG	6,736,679 ~ 6,736,894 bp	58	–
TBL1Y (sY2228)	CTCTGTGTCACCCCCTGC	GGAGAAAAGGAAAAGAGCCAGTA	6,910,077 ~ 6,910,300 bp	58	–
PRKY (sY1817)	GGAGCTAGAAGGAAAAGCATGA	GGCTGGAGGCTGATCATGAT	7,246,851 ~ 7,247,177 bp	60	+
G66267 (sY2183)	CCGTGGAGTGCTACACAGAC	TGCTTATGATTATGGCCTCCA	8,668,480 ~ 8,668,754 bp	60	+
TTTY20 (sY1249)	ACATGGGATCACAGGCTACC	TTTTTGAGGGACTTTCAGCTTC	9,170,480 ~ 9,170,945 bp	60	+
G75495 (sY1250)	TTTTTCTAACCTTGCCTGCG	TGCAGAGAAGCAGCCTACAA	9,399,782 ~ 9,400,274 bp	60	+
G75489 (sY1243)	ATCTGCACACTTGGGTAGGC	GAGGAAATGCAGAATTTGGG	9,465,779 ~ 9,466,271 bp	60	+
G75490 (sY1244)	GCTACTTGTGAATCACGCCA	TGCATATTTCGAAGCATTGTC	9,756,903 ~ 9,757,402 bp	58	–

XPBP1–XPBP4 are named in this study and loci and the corresponding primers
[a], Physical length from the Xp/Yp telomere (according to GRCh37). AT: annealing temperature (°C)
The (+) and (–) symbols represent the presence and the absence of the examined loci, respectively.

was determined to reside within a 246 bp homologous segment at the *PRKX/PRKY* "hot spot A", by sequencing with the primers shown in Table 2 (Fig. 2B).

Discussion

We identified a 45,X-TDSD patient with Xp;Yp translocation. To our knowledge, this is the third case with this condition. Consistent with such rarity, the frequency of 45,X-TDSD with Xp;Yp translocation has been estimated as ~1 of 6×10^7 livebirths, on the basis of the prevalence of loss of maternally derived X chromosome and that of aberrant Xp;Yp translocation during paternal meiosis [1].

The precise Xp;Yp translocation fusion point was determined to reside within a 246 bp segment at the "hot spot A". Although the precise structure of the paternal Y chromosome was not examined because of his refusal for genetic studies other than G-banding, the results argue for the occurrence of aberrant translocation between a normal X chromosome and a Y chromosome with a paracentric Yp inversion involving *PRKY* during paternal meiosis (Fig. 2A) [7, 9, 10]. Thus, the results would provide further support for the notion that a paracentric Yp inversion constitute an underlying factor for the generation of *PRKX/PRKX*-mediated Xp;Yp translocation [7]. In addition, the common ~3.5 Mb Yp inversion mediated by long inverted repeats appears to be present in a certain fraction of Japanese males as well as in ~one-third of European males [7, 8].

Precise Xp;Yp translocation fusion points have been determined at least in a single 45,X-TDSD patient and seven 46,XX-TDSD patients of European origin [4-6], although the presence of a paracentric Yp inversion has been shown in only one of the eight patients [6, 7]. Notably, the fusion points reside at the "hot spot A" in six of the eight patients and at the "hot spot B" in the remaining two patients [4-6]. Furthermore, the fusion point at the "hot spot A" appears to be identical in our patient and four of the six patients reported in the literature [5, 6]. Thus, the 246 bp homologous segment would be regarded as the "remarkable hot spot" for the unbalanced Xp;Yp translocations in males with a paracentric Yp inversion.

The genetic findings are primarily consistent with clinical phenotypes of this patient. Indeed, male sex development is compatible with the presence of *SRY* [11], CDPX1 phenotype (*e.g.*, stippled calcifications, depressed nasal bridge, and hearing loss) is ascribed to loss of *ARSE* [12], and growth failure and relatively short limbs are explainable by *SHOX* haploinsufficiency and chromosome imbalance as well as loss of *ARSE* [12-14]. Although this patient had no Turner-like soft tissue and visceral features, this would also be compatible with the structure of the der(X) chromosome. It has been suggested that such soft tissue and visceral features are deformational consequences

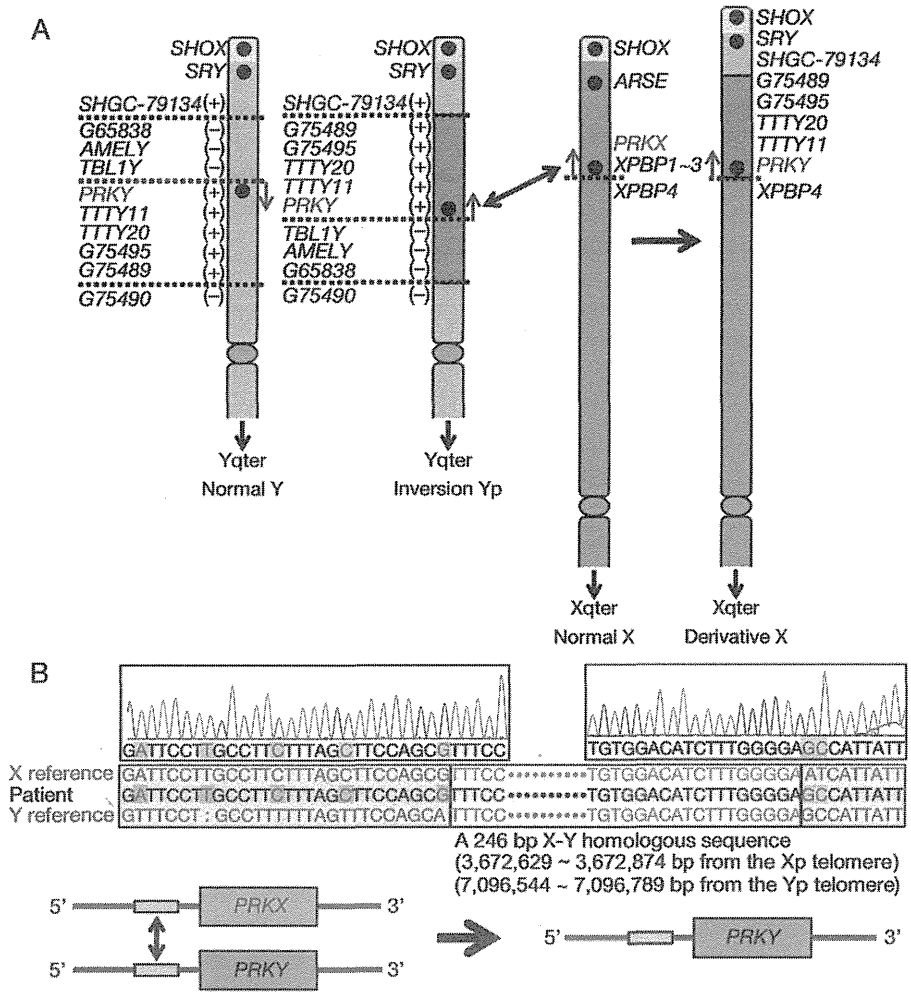

Fig. 2 *PRKX-PRKY*-mediated translocation in the presence of a paracentric Yp inversion.
(A) Schematic representation of the aberrant translocation. The yellow, the pink, the blue, and the green segments denote the short arm pseudoautosomal region, the X-differential region, the Y-differential region, and the Y-differential inverted region, respectively. The (+) and (–) symbols indicate the presence and absence of the loci examined by standard PCR analysis. The data of the Y-specific loci is explained by a single breakpoint, on the assumption of a paracentric Yp inversion in the father. The red arrow indicates the transcriptional direction of *PRKX*, and the blue arrow denotes the transcriptional direction of *PRKY* that is aligned in the same orientation as *PRKX* in the presence of the Yp inversion.
(B) Determination of the translocation fusion point at the "hot spot A" in the 5' region of *PRKX/PRKY* of this patient. Direct sequencing of the long PCR product obtained with an X-specific and a Y-specific primer has shown the presence of X-specific five nucleotides (highlighted with red letters and yellow background) in the centromeric portion and the Y-specific two nucleotides (highlighted with blue letters and yellow background) in the telomeric portion. Thus, the translocation fusion point is located within an X-Y homologous 246 bp segment (indicated by a yellow rectangle) between the X-compatible sequence (indicated by a red rectangle) and the Y-compatible sequence (indicated by a blue rectangle), as illustrated in the below schema.

Table 2 Primers utilized in the determination of the translocation fusion point

	Primer sequence (5' → 3')	Primer position[a]	AT
Long PCR			
X-specific region	CAGTGGATTTAGCTCAGAGGCAGAGAAT	3,673,743 ~ 3,673,770 bp	66
Y-specific region	GCTGGAGAGCTGAAAAGCAATGAGATAG	7,100,894 ~ 7,100,921 bp	66
Direct sequencing of the long PCR product			
X-specific boundary	AGCCTGGGTGACAGAGAAAG	3,672,963 ~ 3,672,982 bp	58
Y-specific boundary	ACTACCTGGGGCCACTTTCT	7,096,924 ~ 7,096,943 bp	58

[a] Physical length from the Xp/Yp telomere (according to GRCh37). AT: annealing temperature (°C)

explained as a malformation sequence initiated by lymphatic hypoplasia [15], and that lymphatic hypoplasia is caused by haploinsufficiency of a putative lymphogenic gene located between *DMD* and *MAOA* at the middle part of Xp and between *DYS255* and *PABY* at the distal part of Yp [16, 17]. Since the *DYS255–PABY* region resides distal to the inverted Yp portion, it is predicted that the putative Y-linked lymphogenic gene is translocated onto the der(X) chromosome, so that the putative lymphogenic gene is present in two copies in this patient, as in normal individuals.

In summary, the present results argue for the presence of rare 45,X-TDSD with Xp;Yp translocation, and for a critical role of a common paracentric Yp inversion in the occurrence of *PRKX/PRKY*-mediated Xp;Yp translocation.

Acknowledgments

This work was Supported in part by Grants-in-Aid for Scientific Research on Innovative Areas (22132004-A01) from the Ministry of Education, Culture, Sports, Science and Technology, by Grant for Research on Intractable Diseases from the Ministry of Health, Labor and Welfare (H24-048), and by Grants from National Center for Child Health and Development (23A-1 and 24-7).

Disclosure Summary

All authors have nothing to disclose.

References

1. Weil D, Portnoï MF, Levilliers J, Wang I, Mathieu M, et al. (1993) A 45,X male with an X;Y translocation: implications for the mapping of the genes responsible for Turner syndrome and X-linked chondrodysplasia punctata. *Hum Mol Genet* 2: 1853–1856.
2. Stuppia L, Calabrese G, Borrelli P, Gatta V, Morizio E, et al. (1999) Loss of the SHOX gene associated with Leri-Weill dyschondrosteosis in a 45,X male. *J Med Genet* 36: 711–713.
3. Chernykh VB, Vyatkina SV, Antonenko VG, Shilova NV, Zolotukhina TV, et al. (2008) Unique mosaic X/Y translocation/insertion in infant 45,X male. *Am J Med Genet A* 146A: 3195–3197.
4. Weil D, Wang I, Dietrich A, Poustka A, Weissenbach J, et al. (1994) Highly homologous loci on the X and Y chromosomes are hot-spots for ectopic recombinations leading to XX maleness. *Nat Genet* 7: 414–419.
5. Wang I, Weil D, Levilliers J, Affara NA, de la Chapelle A, et al. (1995) Prevalence and molecular analysis of two hot spots for ectopic recombination leading to XX maleness. *Genomics* 28: 52–58.
6. Schiebel K, Winkelmann M, Mertz A, Xu X, Page DC, et al. (1997) Abnormal XY interchange between a novel isolated protein kinase gene, PRKY, and its homologue, PRKX, accounts for one third of all (Y+)XX males and (Y–)XY females. *Hum Mol Genet* 6: 1985–1989.
7. Jobling MA, Williams GA, Schiebel GA Pandya GA, McElreavey GA, et al. (1998) A selective difference between human Y-chromosomal DNA haplotypes. *Curr Biol* 8: 1391–1394.
8. Tilford CA, Kuroda-Kawaguchi T, Skaletsky H, Rozen S, Brown LG, et al. (2001) A physical map of the human Y chromosome. *Nature* 409: 943–945.
9. Sharp A, Kusz K, Jaruzelska J, Tapper W, Szarras-Czapnik M, et al. (2005) Variability of sexual phenotype in 46,XX(SRY+) patients: the influence of spreading X inactivation versus position effects. *J Med Genet* 42: 420–427.
10. McElreavey K, Cortes LS (2001) X-Y translocations and sex differentiation. *Semin Reprod Med* 19: 133–139.
11. Sinclair AH, Berta P, Palmer MS, Hawkins JR, Griffiths BL, et al. (1990) A gene from the human sex-determining region encodes a protein with homology to a conserved DNA-binding motif. *Nature* 346: 240–244.
12. Franco B, Meroni G, Parenti G, Levilliers J, Bernard L, et al. (1995) A cluster of sulfatase genes on Xp22.3: mutations in chondrodysplasia punctata (CDPX) and implications for warfarin embryopathy. *Cell* 81: 15–25.
13. Ogata T, Matsuo N (1993) Sex chromosome aberrations and stature: deduction of the principal factors involved in the determination of adult height. *Hum Genet* 91: 551–562.
14. Rao E, Weiss B, Fukami M, Rump A, Niesler B, et al. (1997) Pseudoautosomal deletions encompassing a novel homeobox gene cause growth failure in idiopathic short stature and Turner syndrome. *Nat Genet* 16: 54–63.
15. Ogata T, Matsuo N (1995) Turner syndrome and female sex chromosome aberrations: deduction of the principal factors involved in the development of clinical features. *Hum Genet* 95: 607–629.
16. Ogata T, Muroya K, Matsuo N, Shinohara O, Yorifuji T, et al. (2001) Turner syndrome and Xp deletions: clinical and molecular studies in 47 patients. *J Clin Endocrinol Metab* 86: 5498–5508.
17. Ogata T, Tyler-Smith C, Purvis-Smith S, Turner G (1993) Chromosomal localisation of a gene(s) for Turner stigmata on Yp. *J Med Genet* 30:918–922.

Genomic Basis of Aromatase Excess Syndrome: Recombination- and Replication-Mediated Rearrangements Leading to *CYP19A1* Overexpression

Maki Fukami, Takayoshi Tsuchiya, Heike Vollbach, Kristy A. Brown, Shuji Abe, Shigeyuki Ohtsu, Martin Wabitsch, Henry Burger, Evan R. Simpson, Akihiro Umezawa, Daizou Shihara, Kazuhiko Nakabayashi, Serdar E. Bulun, Makio Shozu, and Tsutomu Ogata*

Context: Genomic rearrangements at 15q21 have been shown to cause overexpression of *CYP19A1* and resultant aromatase excess syndrome (AEXS). However, mutation spectrum, clinical consequences, and underlying mechanisms of these rearrangements remain to be elucidated.

Objective: The aim of the study was to clarify such unsolved matters.

Design, Setting, and Methods: We characterized six new rearrangements and investigated clinical outcome and local genomic environments of these rearrangements and of three previously reported duplications/deletions.

Results: Novel rearrangements included simple duplication involving exons 1–10 of *CYP19A1* and simple and complex rearrangements that presumably generated chimeric genes consisting of the coding region of *CYP19A1* and promoter-associated exons of neighboring genes. Clinical severities were primarily determined by the copy number of *CYP19A1* and the property of the fused promoters. Sequences at the fusion junctions suggested nonallelic homologous recombination, nonhomologous end-joining, and replication-based errors as the underlying mechanisms. The breakpoint-flanking regions were not enriched with GC content, palindromes, noncanonical DNA structures, or known rearrangement-associated motifs. The rearrangements resided in early-replicating segments.

Conclusions: These results indicate that AEXS is caused by duplications involving *CYP19A1* and simple and complex rearrangements that presumably lead to the usage of cryptic promoters of several neighboring genes. Our data support the notion that phenotypes depend on the dosage of *CYP19A1* and the characteristics of the fused promoters. Furthermore, we show that the rearrangements in AEXS are generated by both recombination- and replication-mediated mechanisms, independent of the known rearrangement-inducing DNA features or late-replication timing. Thus, AEXS represents a unique model for human genomic disorders. (*J Clin Endocrinol Metab* 98: E2013–E2021, 2013)

Aromatase excess syndrome (AEXS; MIM no. 139300) is a rare autosomal dominant disorder that causes prepubertal- or peripubertal-onset gynecomastia, hypogonadotropic hypogonadism, advanced bone age, and short adult height in male patients (1, 2). Female patients are usually asymptomatic, although macromastia, irregular menses, and short stature have been reported in a few individuals (2). AEXS results from excessive expression of the aromatase gene *CYP19A1* on chromosome 15q21.2 (NM_000103) (1). *CYP19A1* comprises 11 noncoding exons 1 that function as tissue-specific promoters (exons I.1, IIa, I.8, I.4, I.5, I.7, 1f, I.2, I.6, I.3, and PII), and nine coding exons (exons 2–10) (3, 4). We and other groups have identified various chromosomal rearrangements at

ISSN Print 0021-972X ISSN Online 1945-7197
Printed in U.S.A.

Received June 13, 2013. Accepted September 19, 2013.
First Published Online September 24, 2013

For editorial see page 4676

* Author affiliations are shown at the bottom of the next page.

Abbreviations: AEXS, aromatase excess syndrome; CGH, comparative genomic hybridization.

15q21 in patients with AEXS (1, 2, 5). These rearrangements included duplications that encompassed seven of the 11 noncoding exons 1 of *CYP19A1* and deletions and inversions that generated chimeric genes consisting of coding exons of *CYP19A1* and promoter-associated exons of neighboring genes. Genotype-phenotype analysis has indicated that clinical severities primarily depend on the functional properties of the fused promoters. These findings provide a novel example of gain-of-function mutations resulting from submicroscopic genomic rearrangements.

Rearrangements in the human genome are known to be generated by recombination-based mechanisms, namely, nonallelic homologous recombination and nonhomologous end-joining, and by replication-based mechanisms (6–9). Of these, nonallelic homologous recombination results from unequal crossover between two homologous sequences, usually on the same but sometimes on different chromosomes (10). Nonallelic homologous recombination accounts for most of the recurrent simple deletions and duplications in the human genome and represents the most common abnormality involved in human genomic disorders (9–11). Nonhomologous end-joining occurs as a result of double-strand DNA breakage and subsequent ligation of the two broken DNA ends (12). Nonhomologous end-joining often underlies nonrecurrent simple deletions associated with short nucleotide stretches at the fusion junctions (9–12). Replication-based mechanisms are caused by aberrant template switching during replication and can produce both simple and complex rearrangements that carry microhomologies at the fusion junctions (8, 9, 13). Previous studies have indicated that nonallelic homologous recombination, nonhomologous end-joining, and replication-based mechanisms are facilitated by various local DNA features including high GC content and palindromes (10, 14–16). Highly similar sequences widely spread in the genome ("repetitive elements"), such as *Alu*, LINE1, and MIR, can mediate the occurrence of genomic rearrangements (12). Non-B structures, ie, DNA conformations that differ from the canonical Watson-Crick right-handed double helix, and specific short sequence motifs and tri/tetranucleotides have also been suggested as local genomic stimulants (14–22). Furthermore, replication timing of each chromosomal region appears to determine the frequency of rearrangements; nonallelic homologous recombination preferentially occurs in DNA segments that replicate in early S phase (early-replicating segments), whereas nonhomologous end-joining and replication-based errors frequently appear in late-replicating segments (23).

At present, the underlying mechanisms of the AEXS-associated rearrangements remain largely unknown. Although sequence analysis of the fusion junctions has indicated that nonallelic homologous recombination and nonhomologous end-joining—and possibly replication-based mechanisms as well—are involved in the formation of simple duplications and deletions in AEXS (5), the molecular basis of inversions remains to be determined. Here, we characterized the fine genomic structures of six rearrangements involved in AEXS. Furthermore, we investigated clinical consequences and local genomic environments of the six rearrangements and of three previously reported duplications/deletions.

Patients and Methods

Patients

This study consisted of six cases (cases 1–6) ascertained by prepubertal- or peripubertal-onset gynecomastia. Clinical findings of cases 1–6 are summarized in Table 1. Cases 1–4 are hitherto unreported. Cases 5 and 6 have been described previously, although the genomic structure remains to be determined (1, 2). Cases 1–3 and 5–6 had a 46,XY karyotype, whereas case 4 had a 46,XY inv (9) karyotype that is known as a normal variant. Case 2 had a brother with prepubertal-onset gynecomastia, a sister with premature thelarche, and a father and several paternal relatives with advanced bone age and/or short stature. Case 6 had a son with prepubertal-onset gynecomastia. There was no family history of AEXS in the remaining cases. This study was approved by the Institutional Review Board Committee at the National Center for Child Health and Development. Written informed consent was obtained from the patients and/or their parents.

Copy-number analyses

Leukocyte genomic DNA samples were obtained from cases 1–6, the parents and siblings of case 2, and the son of case 6. Genomic abnormalities involving *CYP19A1* exons and/or its flanking regions were examined by comparative genomic hybridization (CGH) using a custom-made oligoarray or a catalog human array (4 × 180K format, ID 030700 or G4449A; Agilent Technologies). The procedures were performed as described previously (5).

Department of Molecular Endocrinology (M.F., T.T., D.S., T.O.), National Research Institute for Child Health and Development, 157-8535 Tokyo, Japan; Department of Pediatrics (T.T.), Dokkyo Medical University Koshigaya Hospital, 343-8555 Koshigaya, Japan; Department of Pediatrics and Adolescent Medicine (H.V., M.W.), University Medical Center Ulm, 89081 Ulm, Germany; Metabolism and Cancer Laboratory (K.A.B., H.B., E.R.S.), Prince Henry's Institute, Monash Medical Centre, Clayton, 3168 VIC, Australia; Department of Pediatrics (S.A.), Hakodate Goryoukaku Hospital, 040-8611 Hakodate, Japan; Department of Pediatrics (S.O.), Kitasato University School of Medicine, 252-0375 Kanagawa, Japan; Department of Reproductive Biology (A.U.), Center for Regenerative Medicine, National Institute for Child Health and Development, 157-8535 Tokyo, Japan; Department of Maternal-Fetal Biology (K.N.), National Research Institute for Child Health and Development, 157-8535 Tokyo, Japan; Division of Reproductive Biology Research (S.E.B.), Department of Obstetrics and Gynecology, Feinberg School of Medicine, Northwestern University, Chicago, 60611 Illinois; Department of Reproductive Medicine (M.S.), Graduate School of Medicine, Chiba University, 260-8670 Chiba, Japan; and Department of Pediatrics (T.O.), Hamamatsu University School of Medicine, 431-3192 Hamamatsu, Japan

Table 1. Phenotypic and Endocrine Findings of Cases 1–6

	Case 1	Case 2	Case 3	Case 4	Case 5	Case 6
Genomic rearrangement	Duplication	Deletion	Complex	Complex	Complex	Complex
Age at examination, y	10	8 (18)[a]	15	13	17	36
Phenotypic findings						
Gynecomastia (Tanner stage)	**2–3**	**3**	**4–5**	**3–4**	**Severe**	**Severe**
Onset of gynecomastia, y	**7**	Unknown	**8**	**11**	**7**	**5**
Mastectomy	No	**Yes**	**Yes**	No	**Yes**	**Yes**
Testis, mL	6	N.E.	15	12	Normal	Normal
Pubic hair (Tanner stage)	None	None	3–4	4	N.D.	Normal
Facial hair	None	None	None	Scarce	Scarce	**None**
Final height	Unknown	Unknown	−0.9 SD	Unknown	**<1%ile**	**<1%ile**
Bone age, y[b]	**13.0**	**13.5**	N.E.	**18.0**	N.E.	N.E.
Fertility (spermatogenesis)	Unknown	Unknown	Yes	Unknown	Unknown	Yes
Endocrine findings[c]						
At diagnosis						
LH, mIU/mL	<0.1 (0.4–1.6) → 0.4 (10.9–20.6)[d]		2.4 (1.6–3.5)	1.3 (1.6–3.5) → 24.9 (21.7–39.5)[d]	4.3 (1.4–9.2)	1.7 (1.4–9.2)
FSH, mIU/mL	0.3 (1.7–4.2) → 1.6 (4.6–10.8)[d]		<1.0 (4.2–8.2)	0.6 (4.2–8.2) → 2.1 (11.2–17.3)[d]	2.7 (2.0–8.3)	1.5 (4.2–8.2)
T, ng/mL	0.06 (0.4–1.1) → 3.6 (>2.0)[e]	2.6 (2.8–7.0)	0.7 (2.8–7.0)	1.5 (2.8–7.0)	2.3 (2.8–7.0)	3.2 (2.8–7.0)
E_1, pg/mL				**111** (14–50)	**556** (15–32)	**903** (15–32)
E_2, pg/mL	**14** (<10)	**65** (10–35)	**406** (15–50)	**43** (2–30)	**392** (10–35)	**223** (10–35)
On AI treatment						
LH, mIU/mL	0.5 (0.4–1.6) → 7.3 (10.9–20.6)[d]	**44.8** (0.7–5.7)[f]	**4.7** (1.6–3.5)		8.9 (1.4–9.2)	2.9 (1.4–9.2)
FSH, mIU/mL	1.7 (1.7–4.2)→ 3.2 (4.6–10.8)[d]	**34.9** (2.0–8.3)[f]	2.5 (4.2–8.2)		5.6 (2.0–8.3)	5.6 (4.2–8.2)
T, ng/mL	0.9 (0.4–1.1)	**8.6** (2.8–7.0)	6.9 (2.8–7.0)		5.3 (2.8–7.0)	**10.7** (2.8–7.0)
E_1, pg/mL					**89** (15–32)	27 (15–32)
E_2, pg/mL	<10 (<10)	6 (10–35)	13 (15–50)		**59** (10–35)	**68** (10–35)
Reference	Present study	Present study	Present study	Present study	Ref. 1	Ref. 1

Abbreviations: AI, aromatase inhibitor; E_1, estrone; E_2, estradiol; N.D., not described; N.E., not examined. Abnormal clinical findings are boldfaced. Hormone values below the reference range (shown in parentheses) are underlined, and those above the reference range are boldfaced. Conversion factors to the SI unit: LH, 1.0 (IU/L); FSH, 1.0 (IU/L); E_1, 3.699 (pmol/L); E_2, 3.671 (pmol/L); and T, 3.467 (nmol/L).

[a] Physical examination and endocrine studies were carried out at 8 and 18 years of age, respectively.

[b] Assessed by the Tanner-Whitehouse 2 method standardized for Japanese or by the Greulich-Pyle method constructed for Caucasians.

[c] Evaluated by age-matched male reference data.

[d] GnRH stimulation tests (100 μg/m^2, maximum 100 μg bolus iv; blood sampling at 0, 30, 60, 90, and 120 min).

[e] Human chorionic gonadotropin stimulation tests (3000 IU/m^2, maximum 5000 IU im for 3 consecutive days; blood sampling on d 1 and 4).

[f] Increased levels of LH and FSH during AI treatment may be associated with low E_2 levels (24).

Characterization of the genomic structures of rearrangements

Breakpoints of the rearrangements were determined by direct sequencing of the PCR-amplified DNA fragments harboring the fusion junctions. PCRs were carried out using a number of primer pairs for various genomic positions around *CYP19A1*. The sequences of the primers utilized in the present study are available upon request. To confirm the formation of a chimeric gene in a case with a complex rearrangement, we performed RT-PCR using leukocyte mRNA and primers annealing to exon 2 of *CYP19A1* and exons of neighboring genes. The presence or absence of promoter-associated histone marks in the fused exons was analyzed using the UCSC genome browser (http://genome.ucsc.edu/).

Genotype-phenotype analysis

We performed genotype-phenotype analyses in cases 1–6 and in 18 patients identified in our previous study (5).

DNA sequences at the fusion junctions

To clarify the underlying mechanisms of the rearrangements, we examined the presence or absence of microhomologies and short nucleotide stretches at the fusion junctions. In addition, we searched for repeat elements around the breakpoints using Repeatmasker (http://www.repeatmasker.org).

Genomic environments around the breakpoints

We studied the frequencies of known rearrangement-inducing DNA features in the breakpoint-flanking regions. In silico analyses were carried out in the 300-bp regions at the proximal and distal sides of each breakpoint. We also examined control regions (n = 53) randomly selected at an interval of 1.5 Mb from the entire 15q (Supplemental Table 1, published on The Endocrine Society's Journals Online web site at http://jcem.endojournals.org). We calculated the average GC content using GEECEE (http://emboss.bioinformatics.nl/cgi-bin/emboss/geecee) and searched for palindromes using PALINDROME (http://mobyle.pasteur.fr/cgi-bin/portal.py#forms::palindrome) and Non-B structures using Non-B DB (http://nonb.abcc.ncifcrf.gov). Examined Non-B structures included direct repeats, inverted repeats (cruciforms), mirror repeats, A-phased repeats, G-quadruplex repeats, short tandem repeats, and Z-DNA motifs (17). The presence or absence of the 10 specific sequence motifs and two tri/tetranucleotides implicated in rearrangements in various chromosomal regions (14, 18–22) were analyzed using Fuzznuc (http://emboss.bioinformatics.nl/cgi-bin/emboss/fuzznuc).

Replication timing analysis

We analyzed whether the rearrangements at 15q21 have occurred at a specific timing of S phase (23). Replication timing profiles of the approximately 10-Mb genomic interval around *CYP19A1* were evaluated using 92 datasets currently available in

Table 2. Genomic Rearrangements in Cases 1–6

	Rearrangement	Genomic Abnormality	Affected Genes[a]
Case 1	Simple	Simple duplication	*CYP19A1, TNFAIP8L3, AP4E1*
Case 2	Simple	Simple deletion	*CYP19A1, GLDN, DMXL2*
Case 3[b]	Complex	Multiple deletions?	*TMOD3, GLDN, DMXL2?*
Case 4	Complex	Multiple duplications and inversion	*CYP19A1, GLDN, SEMA6D*
Case 5	Complex	Multiple duplications, deletion, and inversion	*TMOD3, DMXL2, TMOD2, LYSMD2, SCG3*
Case 6	Complex	Multiple deletions and inversion	*CGNL1, CYP19A1*

[a] Genes involved in the deletion or duplication. Genes affected by copy-number-neutral inversions are not shown.

[b] Genomic structure of the rearrangement in case 3 remains to be characterized.

the ReplicationDomain database (http://www.replicationdomain.com/replication_timing.php).

Statistical analyses

Statistical significance of the average GC content between the breakpoint-flanking and control regions was analyzed by Student's *t* test. Differences in the frequencies of other rearrangement-inducing DNA features were examined by Fisher's exact probability test. $P < .05$ was considered significant.

Results

Copy-number alterations in cases 1–6

CGH analyses indicated heterozygous genomic rearrangements involving *CYP19A1* and/or its neighboring genes; ie, an approximately 0.4-Mb duplication involving *CYP19A1*, *TNFAIP8L3*, and *AP4E1* in case 1; an approximately 0.3-Mb deletion affecting *DMXL2*, *CYP19A1*, and *GLDN* in case 2; an approximately 80-kb deletion involving *TMOD3* and an approximately 250-kb deletion involving *DMXL2* and *GLDN* in case 3; an approximately 130-kb duplication involving *GLDN* and *CYP19A1* and an approximately 340-kb duplication involving *SEMA6D* at a position of approximately 3.6 Mb distant from *CYP19A1* in case 4; an approximately 370-kb duplication involving *TMOD3*, *TMOD2*, *LYSMD2*, *SCG3*, and *DMXL2*, and a 3- to 35-kb deletion between *DMXL2* and *GLDN* in case 5; and an approximately 3.5-kb deletion in the promoter region of *CYP19A1* in case 6 (Table 2 and Figure 1). The deletion in case 5 could not be narrowed down because of the absence of CGH probes around the breakpoints. The father and siblings of case 2 and the son of case 6 carried the same abnormalities as the probands.

Genomic structures of six rearrangements

We were able to characterize all fusion junctions in cases 1, 2, and 6 and one of the multiple junctions in cases 4 and 5 (Table 3, Supplemental Table 2, and Figure 2). The remaining breakpoints could not be determined due to the low quality of the DNA samples, the presence of long repetitive sequences around the breakpoints, or the complex structures of the rearrangements. In case 1, we identified a 387 622-bp tandem duplication involving six of the 11 exons 1 (exons I.7, 1f, I.2, I.6, I.3, and PII) and all coding exons of *CYP19A1*, together with all exons of *TNFAIP8L3* and *AP4E1*. In case 2, we detected a 303 624-bp deletion involving six of the *CYP19A1* exons 1 (exons I.1, IIa, I.8, I.4, I.5, and I.7), all exons of *GLDN*, and *DMXL2* exons 2–43. In case 4, we identified two duplications: an approximately 130-kb duplication encompassing all noncoding exons 1 and coding exons 2–3 of *CYP19A1* and *GLDN* exon 1, and an approximately 340-kb duplication involving *SEMA6D* exons 1–3. PCR products were obtained with a primer pair for *GLDN* intron 1 and *SEMA6D* intron 3 (P5 and P6 in Figure 2A), indicating that the approximately 3.6-Mb genomic interval harboring *GLDN* exon 1, all noncoding and coding exons of *CYP19A1*, and *SEMA6D* exons 4–20 was inverted. In addition, we analyzed mRNA of case 4 and detected a chimeric clone composed of *CYP19A1* exon 2 and *SEMA6D* noncoding exon 3 (Supplemental Figure 1). Thus, although we could not determine the fusion junctions of the duplication, these data imply that the rearrangement was caused by an inversion of an approximately 3.6-Mb region and a duplication of the telomeric part of the inverted DNA fragment. In case 5, we identified an approximately 370-kb duplication containing *TMOD3* exon 1, *DMXL2* exons 1–29, and all exons of *TMOD2*, *LYSMD2*, and *SCG3*. PCR products were obtained with a primer pair for *TMOD3* intron 1 and the downstream region of *GLDN* (P7 and P8), indicating that the approximately 370-kb region was duplicated and inserted into the genome in a reverse direction. The small deletion between *DMXL2* and *GLDN* detected by CGH could not be characterized because of the presence of long repetitive sequences around the breakpoints. In case 6, we identified a complex deletion–inversion–deletion rearrangement: a 202-bp deletion within *CGNL1* intron 1, an approximately 6.1-Mb inversion encompassing *CGNL1* exon 1, eight of the *CYP19A1* exons 1 (exons I.1, IIa, I.8, I.4, I.5, I.7, 1f, and I.2), and ≥25 genes, and a 3476-bp deletion within *CYP19A1* intron 1.

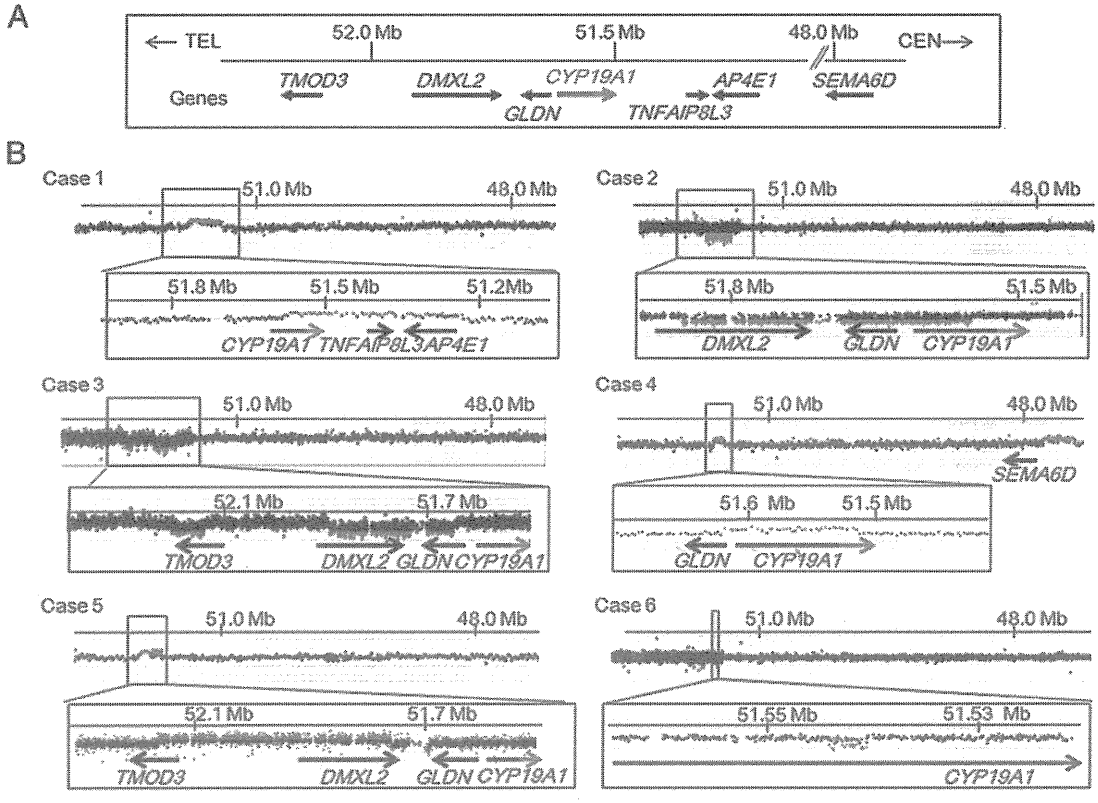

Figure 1. Copy-number analyses in cases 1–6. A, Schematic representation of the normal genomic structure around *CYP19A1*. The arrows indicate genomic positions and transcriptional direction of genes (5′→3′). For *CYP19A1*, the dark and light blue lines denote the genomic regions for noncoding exons 1 and coding exons 2–10, respectively. Genomic positions refer to Human Genome Database (hg19, build 37). Only genes around the fusion junctions are shown. B, CGH analyses in the six cases. The black, red, and green dots denote signals indicative of the normal, increased (>+0.5) and decreased (<−1.0) copy-numbers, respectively.

Phenotypic consequences of the six new and three previously reported rearrangements

We studied genotype-phenotype correlation in cases 1–6 and 18 previously reported patients (four patients from families A–B with simple duplications involving the *CYP19A1* promoter region, and 14 patients from families C–F with *DMXL2-CYP19A1* chimeric genes) (*5*). The results are summarized in Table 4. First, clinical severities were relatively mild in case 1 and patients from families A–B with simple duplications, obviously severe in cases 5 and 6 with complex rearrangements, and moderate in the remaining cases/patients with simple deletions or complex rearrangements. Second, among cases/patients with simple duplications, case 1 showed earlier onset of gyneco-

Table 3. Fusion Junctions in Cases 1–6

	No. of Fusion Junctions	No. of Fusion Junctions Characterized in This Study[a]	Sequences at the Fusion Junctions		Predicted Mechanism
			Microhomology	Nucleotide Stretch	
Case 1	1	1	Yes (4 bp)	Yes (2 bp)	RBM
Case 2	1	1	Yes (2 bp)	No	RBM
Case 3[b]	2?	0	Unknown	Unknown	RBM?
Case 4	5	1	Yes (20 bp)	No	RBM
Case 5	3	1	Yes (3 bp)	Yes (5 bp)	RBM
Case 6	2	2	Yes (3 bp)[c]/No	No	RBM

Abbreviation: RBM, replication-based mechanism.

[a] Several breakpoints could not be determined due to low quality of the DNA samples, the presence of long repetitive sequences around the breakpoints, or the complex structures of the rearrangements.

[b] Genomic structure of the rearrangement in case 3 remains to be characterized.

[c] Microhomology was observed at the telomeric junction.

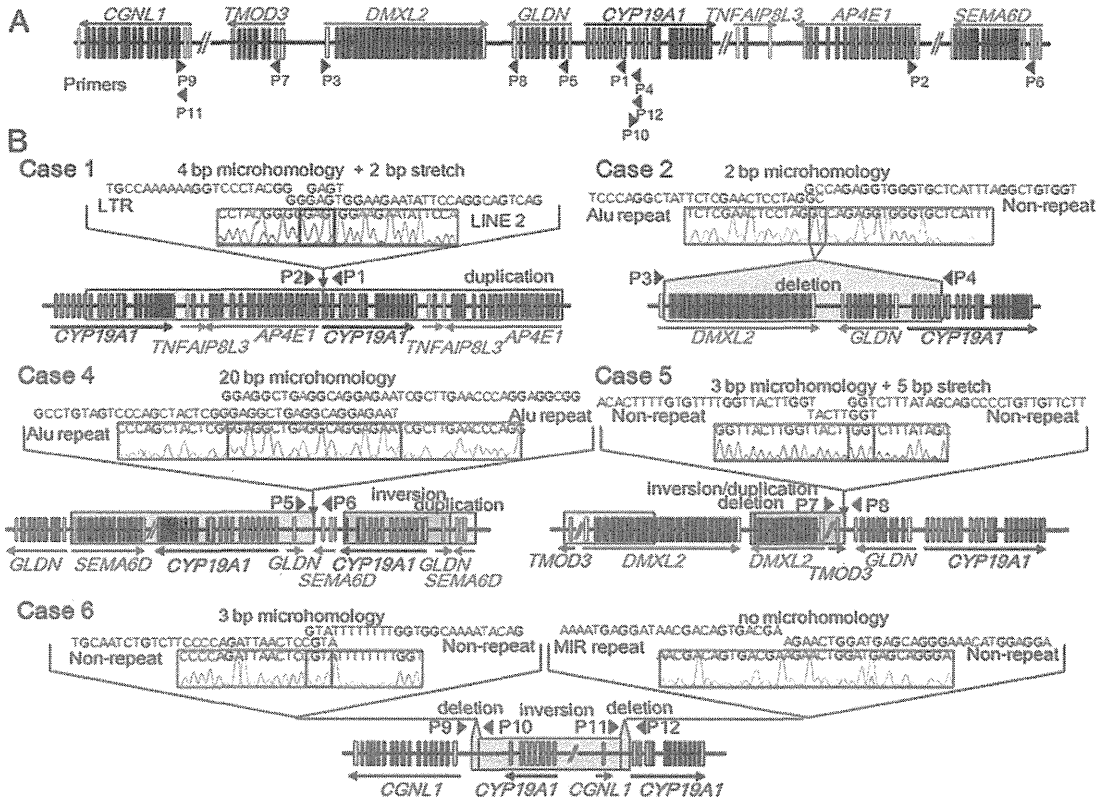

Figure 2. Fine genomic structures of the rearrangements. A, Schematic representation of the normal genomic structure. Arrowheads indicate the positions and the directions (5′→3′) of PCR primers utilized in this study (P1–P12). The open and color-painted boxes denote noncoding and coding exons, respectively. The sizes of the exons, introns, and primers are not drawn to scale. B, Schematic representation of the rearrangements and the DNA sequences at the fusion junctions. The red, blue, and green areas indicate duplications, deletions, and inversions, respectively. P1–P12 indicate the same PCR primers as shown in panel A. The fusion junctions of case 3 were not characterized. For case 4, the precise genomic position of the duplication remains to be clarified.

mastia and more severely advanced bone age than patients from families A–B. Third, among cases/patients with deletions, case 2 manifested milder gynecomastia than case 3 and patients from families C–F. Lastly, among cases/patients with deletions or complex rearrangements, cases 2–4 and patients from families C–F showed milder phenotypes than cases 5 and 6.

DNA sequences at the fusion junctions

We characterized fusion junctions of the rearrangements in cases 1, 2, and 4–6 and in patients from families A–F (Table 3, Supplemental Table 2, and Figure 2). The results indicated the following: 1) nonallelic homologous recombination for the recurrent simple deletions in patients from families D–F that took place between two homologous sequences; 2) nonhomologous end-joining for the nonrecurrent simple deletions in patients from family C that were associated with short nucleotide stretches at the fusion junction; and 3) replication-based mechanisms for the simple and complex aberrations in cases 1, 2, and 4–6, and in patients from families A–B that were accompanied by microhomologies at the fusion junction. Nine of the 18 breakpoints resided within repetitive elements, such as LINE 1, LINE 2, *AluJo*, *AluY*, and *AluSx3*.

Genomic environments around the breakpoints

The average GC content was similar between the breakpoint-flanking and control regions (Supplemental Tables 2 and 3). Furthermore, the frequencies of known rearrangement-inducing DNA features (12, 14, 18–22) did not significantly differ between the breakpoint-flanking and control regions, except for some non-B structures enriched around the breakpoints of the deletions in patients from families D–F (Supplemental Tables 2 and 3).

Replication timing of the 15q21 region

Replication timing analysis indicated that in most cell lines examined, the genomic region around *CYP19A1* is replicated during early S phase (Supplemental Figure 2).

Discussion

We characterized six genomic rearrangements in patients with AEXS (Supplemental Figure 3). In case 1, the tandem duplication seems to have enhanced the transcriptional efficiency of *CYP19A1* in native *CYP19A1*-expressing tissues by increasing the number of transcription start sites. In cases 2–6, the rearrangements are predicted to have

Table 4. Genotype-Phenotype Correlation in Cases 1–6 and Families A–F

Cases/Families[a]	Case 1	Families A and B	Case 2	Case 3[b], Families C–F	Case 4	Case 5	Case 6
Molecular defects							
Predicted mechanism for *CYP19A1* overexpression	Duplication of *CYP19A1* coding exons	Duplication of *CYP19A1* promoters	Chimeric gene formation	Chimeric gene formation	Chimeric gene formation	Chimeric gene formation	Chimeric gene formation
Genes involved in chimeric gene formation	None	None	*DMXL2*	*DMXL2*	*SEMA6D*	*TMOD3*	*CGNL1*
Copy-number of the *CYP19A1* exon 1.4[c]	Normal	Increased	Decreased	Normal	Increased[d]	Normal	Decreased
Clinical findings							
Onset of gynecomastia, y	7	10–13	Unknown	7–12	11	7	5
Gynecomastia (Tanner stage)	2–3	2–3	1–3[e]	3–5	3–4	Severe	Severe
Advanced bone age	Mild	Subtle	Moderate	Mild/ moderate	Severe	N.E.	N.E.

Abbreviation: N.E., not examined.

[a] Cases 1–6 were present cases, whereas families A–F were reported previously (5).

[b] Fine genomic structure of case 3 remains to be characterized.

[c] Exon 1.4 functions as the major promoter in extragonadal tissues.

[d] Duplicated exon 1.4 has been disconnected from the coding exons of *CYP19A1*.

[e] The patient and his father had gynecomastia of Tanner stages 3 and 1, respectively.

created chimeric genes consisting of coding exons of *CYP19A1* and promoter-associated exons of neighboring genes. Actually, the deletions in cases 2 and 3 appear to have permitted splicing between *DMXL2* exon 1 and *CYP19A1* exon 2, as has been shown in the patients with similar deletions (5). Furthermore, the inversion in case 4 was found to produce a chimeric gene consisting of exon 3 of *SEMA6D* and exon 2 of *CYP19A1* (Supplemental Figure 1), and the inversions in cases 5 and 6 have previously been shown to form *TMOD3*- and *CGNL1-CYP19A1* chimeric genes, respectively (2). In this regard, the rearrangements in cases 2–6 have brought not only exons 1 of other genes, but also their flanking regions of >10 kb, to lie near the coding region of *CYP19A1*. Because these flanking regions harbor several enhancer- and promoter-associated histone marks (H3K4Me1 and H3K4Me3) (Supplemental Figure 4), they appear to contain most, if not all, components of cis-regulatory elements. Thus, although we can not examine the actual expression pattern of the chimeric genes, these genes seem to be expressed in a wide range of tissues where the original genes are expressed. These results argue for a broad mutation spectrum of AEXS.

Such diverse genetic basis of AEXS would be relevant to phenotypic variations (Table 4). First, cases/patients with copy-number gains of *CYP19A1* showed milder phenotypes than those with chimeric genes. This is consistent with the limited tissue expression pattern of *CYP19A1* and broad expression patterns of other genes involved in the chimeric gene formation (5, 25). Second, among cases/patients with simple duplications, case 1 showed a more severe phenotype than patients from families A–B. This suggests that tandem duplications encompassing the transcriptional unit, ie, the promoter region plus the coding exons, permit more efficient aromatase protein production than tandem duplications encompassing the promoter region only. Third, among cases/patients with the same *DMXL2-CYP19A1* chimeric gene, case 2 manifested milder phenotypes than case 4 and patients from families C–F. These results can be explained by the difference in the number of *CYP19A1* exons 1, because six of *CYP19A1* exons 1 were deleted in case 2 and all exons 1 were preserved in the remaining cases/patients (Supplemental Figure 5). Fourth, case 4 with a *SEMA6D-CYP19A1* chimeric gene showed a milder phenotype than cases 5 and 6 with a *TMOD3*- and *CGNL1-CYP19A1* chimeric gene, respectively. This is consistent with a tissue expression pattern being broader in *TMOD3* and *CGNL1* than in *SEMA6D* (5, 25). Lastly, cases/patients with *DMXL2-CYP19A1* chimeric genes manifested milder phenotype than cases with a *TMOD3*- or *CGNL1-CYP19A1* chimeric gene. This would primarily be ascribed to the presence or absence of a translational start codon on the fused promoter-associated exons (Supplemental Figure 6). It is likely that *DMXL2-CYP19A1* chimeric mRNAs transcribed by the *DMXL2* promoter preferentially recognize the natural start codon on *DMXL2* exon 1 and undergo nonsense-mediated mRNA decay, and rather exceptional chimeric mRNAs utilize the start codon on *CYP19A1* exon 2 and produce the aromatase protein (5). Such a phenomenon would not be postulated for

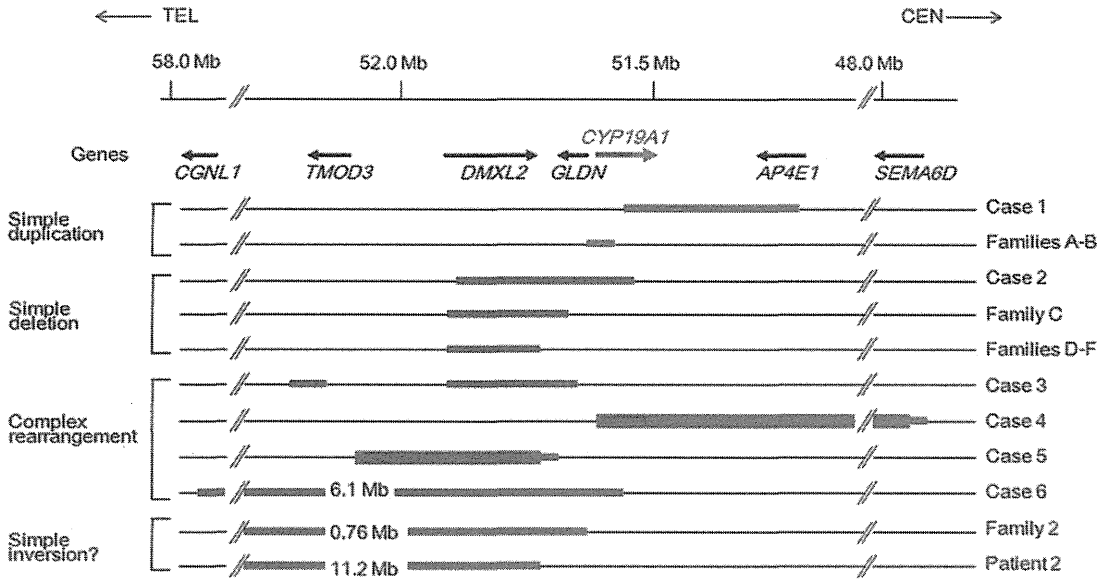

Figure 3. Schematic representation of the 11 rearrangements. Cases 1, 2, and 4–6 are from the present study, and patients from families A–F, patient 2, and patients from family 2 have been reported previously (1, 2, 5). The genomic abnormalities of case 3 were not characterized. The arrows indicate the positions and transcriptional direction of *CYP19A1* and its neighboring genes (5′→3′). Only genes around the fusion junctions are shown. The red, blue, and green lines indicate duplications, deletions, and inversions, respectively. For *CYP19A1*, the dark and light blue lines denote the genomic regions for the noncoding and coding exons, respectively. The inversions of family 2 and patient 2 may be complex rearrangements because copy-number analyses have not been performed in these cases.

the *TMOD3*- and *CGNL1-CYP19A1* chimeric mRNAs because of the absence of a translation start codon on exons 1 of *TMOD3* and *CGNL1*. Taken together, the present study suggests that phenotypic severity is primarily determined by the copy-number of *CYP19A1* and by the expression patterns and structural properties of the fused promoters. It should be pointed out, however, that this conclusion is based on the observation of only a limited number of patients. Phenotypic variation of the patients may be due to low penetrance of the clinical features.

To date, 11 genomic rearrangements have been identified in patients with AEXS (Figure 3). The 11 rearrangements are widely distributed on an approximately 9-Mb region and include simple duplications, deletions, and inversions, as well as complex rearrangements. Of these, the rearrangements in cases 1, 2, and 4–6 and in patients from families A–B are predicted to be replication-based errors (Supplemental Table 2 and Figure 2). Although the short nucleotide stretches at the fusion junctions in cases 1 and 5 may represent "information scars" characteristic of nonhomologous end-joining (9), the complex structures of the rearrangements would be consistent with replication-based mechanisms rather than end-joining (8). However, these rearrangements may result from microhomology-mediated end-joining (26). In contrast, the simple deletions in patients from family C and those in patients from families D–F are compatible with nonhomologous end-joining and nonallelic homologous recombination, respectively (Supplemental Table 2 and Figure 2). These results imply that the genomic region at 15q21 is vulnerable to both recombination- and replication-mediated errors.

In silico analyses revealed that deletions in families D–F due to nonallelic homologous recombination were associated with non-B structures and were located within an early-replicating segment of the genome, whereas the breakpoint-flanking regions of other rearrangements were independent of known rearrangement-inducing DNA features or late-replication timing. These data indicate that there are hitherto unidentified factors that facilitate nonhomologous end-joining and replication-based errors at 15q21. In this regard, it is noteworthy that nine of the 18 breakpoints resided within repetitive elements, and frequencies of *Alu*s (16%) and LINEs (22%) in the breakpoint-flanking regions were slightly higher than expected from the draft human genome (*Alu*, 9.9%; and LINE, 16.1%) (27). An increased number of repetitive sequences was found around the breakpoints of various rearrangements (14, 18, 19, 21), and Boone et al (28) have reported that a high concentration of *Alu* elements may predispose replication-based errors. The presence of various *Alu* family members (*AluJo*, *AluY*, and *AluSx3*) at the fusion junction of our cases supports the notion that moderate sequence similarity between *Alu* elements would be sufficient to provide substrates for replication-based errors (28). Further studies are necessary to clarify the role of repetitive sequences in the formation of rearrangements.

In summary, the present study implies a broad mutation spectrum of AEXS and supports the previously proposed

notion that clinical severities of AEXS are determined by the dosage of the promoter and coding regions of *CYP19A1* and by characters of the fused promoters. We show that rearrangements involved in AEXS can be attributed to nonallelic homologous recombination that is induced by repeats and/or by early-replication timing, and to nonhomologous end-joining and replication-based mechanisms that occur independently of known rearrangement-inducing DNA features or a late-replicating timing. Thus, AEXS represents a unique model for human genomic disorders.

Acknowledgments

Address all correspondence and requests for reprints to: Maki Fukami, MD, Department of Molecular Endocrinology, National Research Institute for Child Health and Development, 2-10-1 Ohkura, Setagaya, Tokyo 157-8535, Japan. E-mail: fukami-m@ncchd.go.jp.

This work was supported by the Grant-in-Aid for Scientific Research on Innovative Areas from the Ministry of Education, Culture, Sports, Science, and Technology; by the Grant-in-Aid for Scientific Research and for Challenging Exploratory Research from the Japan Society for the Promotion of Science; by the Grant for Research on Intractable Diseases from the Ministry of Health, Labor, and Welfare; by grants from the National Center for Child Health and Development; and by grants from the Takeda Foundation and the Daiichi-Sankyo Foundation of Life Science.

Disclosure Summary: The authors have nothing to disclose.

References

1. **Shozu M, Sebastian S, Takayama K, et al.** Estrogen excess associated with novel gain-of-function mutations affecting the aromatase gene. *N Engl J Med.* 2003;348:1855–1865.
2. **Demura M, Martin RM, Shozu M, et al.** Regional rearrangements in chromosome 15q21 cause formation of cryptic promoters for the CYP19 (aromatase) gene. *Hum Mol Genet.* 2007;16:2529–2541.
3. **Bulun SE, Takayama K, Suzuki T, Sasano H, Yilmaz B, Sebastian S.** Organization of the human aromatase p450 (CYP19) gene. *Semin Reprod Med.* 2004;22:5–9.
4. **Demura M, Reierstad S, Innes JE, Bulun SE.** Novel promoter I.8 and promoter usage in the CYP19 (aromatase) gene. *Reprod Sci.* 2008; 15:1044–1053.
5. **Fukami M, Shozu M, Soneda S, et al.** Aromatase excess syndrome: identification of cryptic duplications and deletions leading to gain of function of CYP19A1 and assessment of phenotypic determinants. *J Clin Endocrinol Metab.* 2011;96:E1035–E1043.
6. **Lee C, Iafrate AJ, Brothman AR.** Copy number variations and clinical cytogenetic diagnosis of constitutional disorders. *Nat Genet.* 2007;39:S48–S54.
7. **Lupski JR, Stankiewicz P.** Genomic disorders: molecular mechanisms for rearrangements and conveyed phenotypes. *PLoS Genet.* 2005;1:e49.
8. **Hastings PJ, Ira G, Lupski JR.** A microhomology-mediated break-induced replication model for the origin of human copy number variation. *PLoS Genet.* 2009;5:e1000327.
9. **Gu W, Zhang F, Lupski JR.** Mechanisms for human genomic rearrangements. *Pathogenetics.* 2008;1:4.
10. **Shaw CJ, Lupski JR.** Implications of human genome architecture for rearrangement-based disorders: the genomic basis of disease. *Hum Mol Genet.* 2004;13:R57–R64.
11. **Conrad DF, Bird C, Blackburne B, et al.** Mutation spectrum revealed by breakpoint sequencing of human germline CNVs. *Nat Genet.* 2010;42:385–391.
12. **Chen JM, Cooper DN, Férec C, Kehrer-Sawatzki H, Patrinos GP.** Genomic rearrangements in inherited disease and cancer. *Semin Cancer Biol.* 2010;20:222–233.
13. **Colnaghi R, Carpenter G, Volker M, O'Driscoll M.** The consequences of structural genomic alterations in humans: genomic disorders, genomic instability and cancer. *Semin Cell Dev Biol.* 2011; 22:875–885.
14. **Froyen G, Belet S, Martinez F, et al.** Copy-number gains of HUWE1 due to replication- and recombination-based rearrangements. *Am J Hum Genet.* 2012;91:252–264.
15. **Wang G, Zhao J, Vasquez KM.** Methods to determine DNA structural alterations and genetic instability. *Methods.* 2009;48:54–62.
16. **Kurahashi H, Inagaki H, Ohye T, Kogo H, Kato T, Emanuel BS.** Palindrome-mediated chromosomal translocations in humans. *DNA Repair (Amst).* 2006;5:1136–1145.
17. **Cer RZ, Donohue DE, Mudunuri US, et al.** Non-B DB v2.0: a database of predicted non-B DNA-forming motifs and its associated tools. *Nucl Acids Res.* 2013;41:D94–D100.
18. **Verdin H, D'haene B, Beysen D, et al.** Microhomology-mediated mechanisms underlie non-recurrent disease-causing microdeletions of the FOXL2 gene or its regulatory domain. *PLoS Genet.* 2013;9: e1003358.
19. **Carvalho CM, Zhang F, Liu P, et al.** Complex rearrangements in patients with duplications of MECP2 can occur by fork stalling and template switching. *Hum Mol Genet.* 2009;18:2188–2203.
20. **Kornreich R, Bishop DF, Desnick RJ.** α-Galactosidase A gene rearrangements causing Fabry disease. Identification of short direct repeats at breakpoints in an Alu-rich gene. *J Biol Chem.* 1990;265: 9319–9326.
21. **Vissers LE, Bhatt SS, Janssen IM, et al.** Rare pathogenic microdeletions and tandem duplications are microhomology-mediated and stimulated by local genomic architecture. *Hum Mol Genet.* 2009; 18:3579–3593.
22. **Liu P, Carvalho CM, Hastings PJ, Lupski JR.** Mechanisms for recurrent and complex human genomic rearrangements. *Curr Opin Genet Dev.* 2012;22:211–220.
23. **Koren A, Polak P, Nemesh J, et al.** Differential relationship of DNA replication timing to different forms of human mutation and variation. *Am J Hum Genet.* 2012;91:1033–1040.
24. **Patry G, Jarvi K, Grober ED, Lo KC.** Use of the aromatase inhibitor letrozole to treat male infertility. *Fertil Steril.* 2009;92:829.e1–e2.
25. **Nagase T, Kikuno R, Ishikawa K, Hirosawa M, Ohara O.** Prediction of the coding sequences of unidentified human genes. XVII. The complete sequences of 100 new cDNA clones from brain which code for large proteins in vitro. *DNA Res.* 2000;7:143–150.
26. **Lieber MR.** The mechanism of human nonhomologous DNA end joining. *J Biol Chem.* 2008;283:1–5.
27. **Venter JC, Adams MD, Myers EW, et al.** The sequence of the human genome. *Science.* 2001;291:1304–1351.
28. **Boone PM, Liu P, Zhang F, et al.** Alu-specific microhomology-mediated deletion of the final exon of SPAST in three unrelated subjects with hereditary spastic paraplegia. *Genet Med.* 2011;13:582–592.
29. **Pope BD, Tsumagari K, Battaglia D, et al.** DNA replication timing is maintained genome-wide in primary human myoblasts independent of D4Z4 contraction in FSH muscular dystrophy. *PLoS One.* 2011;6:e27413.
30. **Ryba T, Battaglia D, Chang BH, et al.** Abnormal developmental control of replication-timing domains in pediatric acute lymphoblastic leukemia. *Genome Res.* 2012;22:1833–1844.
31. **Pope BD, Chandra T, Buckley Q, et al.** Replication-timing boundaries facilitate cell-type and species-specific regulation of a rearranged human chromosome in mouse. *Hum Mol Genet.* 2012;21: 4162–4170.

OPEN ACCESS Freely available online

PLOS ONE

Cryptic Genomic Rearrangements in Three Patients with 46,XY Disorders of Sex Development

Maki Igarashi[1☯], Vu Chi Dung[2☯], Erina Suzuki[1], Shinobu Ida[3], Mariko Nakacho[3], Kazuhiko Nakabayashi[4], Kentaro Mizuno[5], Yutaro Hayashi[5], Kenjiro Kohri[5], Yoshiyuki Kojima[5,6], Tsutomu Ogata[1,7], Maki Fukami[1]*

1 Department of Molecular Endocrinology, National Research Institute for Child Health and Development, Tokyo, Japan, **2** Department of Endocrinology, Metabolism and Genetics, The Vietnam National Hospital of Pediatrics, Hanoi, Vietnam, **3** Department of Gastroenterology and Endocrinology, Osaka Medical Center and Research Institute for Maternal and Child Health, Osaka, Japan, **4** Department of of Maternal-Fetal Biology, National Research Institute for Child Health and Development, Tokyo, Japan, **5** Department of Nephro-Urology, Nagoya City University Graduate School of Medical Sciences, Nagoya, Japan, **6** Department of Urology, Fukushima Medical University School of Medicine, Fukushima, Japan, **7** Department of Pediatrics, Hamamatsu University School of Medicine, Hamamatsu, Japan

Abstract

Background: 46,XY disorders of sex development (46,XY DSD) are genetically heterogeneous conditions. Recently, a few submicroscopic genomic rearrangements have been reported as novel genetic causes of 46,XY DSD.

Methodology/Principal Findings: To clarify the role of cryptic rearrangements in the development of 46,XY DSD, we performed array-based comparative genomic hybridization analysis for 24 genetic males with genital abnormalities. Heterozygous submicroscopic deletions were identified in three cases (cases 1–3). A ~8.5 Mb terminal deletion at 9p24.1–24.3 was detected in case 1 that presented with complete female-type external genitalia and mental retardation; a ~2.0 Mb interstitial deletion at 20p13 was identified in case 2 with ambiguous external genitalia and short stature; and a ~18.0 Mb interstitial deletion at 2q31.1–32 was found in case 3 with ambiguous external genitalia, mental retardation and multiple anomalies. The genital abnormalities of case 1 could be ascribed to gonadal dysgenesis caused by haploinsufficiency of *DMRT1*, while those of case 3 were possibly associated with perturbed organogenesis due to a deletion of the *HOXD* cluster. The deletion in case 2 affected 36 genes, none of which have been previously implicated in sex development.

Conclusions/Significance: The results indicate that cryptic genomic rearrangements constitute an important part of the molecular bases of 46,XY DSD and that submicroscopic deletions can lead to various types of 46,XY DSD that occur as components of contiguous gene deletion syndromes. Most importantly, our data provide a novel candidate locus for 46,XY DSD at 20p13.

Citation: Igarashi M, Dung VC, Suzuki E, Ida S, Nakacho M, et al. (2013) Cryptic Genomic Rearrangements in Three Patients with 46,XY Disorders of Sex Development. PLoS ONE 8(7): e68194. doi:10.1371/journal.pone.0068194

Editor: Reiner Albert Veitia, Institut Jacques Monod, France

Received March 7, 2013; **Accepted** May 27, 2013; **Published** July 8, 2013

Funding: This work was supported by the Grant-in-Aid for Scientific Research on Innovative Areas (22132004) from the Ministry of Education, Culture, Sports, Science and Technology, by the Grant for Research on Intractable Diseases from the Ministry of Health, Labor and Welfare, by the Grant-in-Aid for Scientific Research (B) (23390249) and for Young Scientists (B) (24791103) from the Japan Society for the Promotion of Science (JSPS), by the Grant from the Takeda Foundation and by the Grant from National Center for Child Health and Development (23A-1 and 24-7). The funders had no role in study design, data collection and analysis, decision to publish, or preparation of the manuscript.

Competing Interests: The authors have declared that no competing interests exist.

* E-mail: fukami-m@ncchd.go.jp

☯ These authors contributed equally to this work.

Introduction

46,XY disorders of sex development (46,XY DSD) are genetically heterogeneous conditions that result from the impaired production or function of androgens, or from defective organogenesis of external genitalia [1]. To date, several genes such as *SRY*, *AR*, *SRD5A2*, and *SOX9* have been identified as causative genes for 46,XY DSD, although mutations in these genes account for only a minor fraction of the molecular causes of these conditions [1], [2].

Recent advances in microarray technology, including comparative genomic hybridization (CGH) analysis and single nucleotide polymorphism (SNP) genotyping, have enabled researchers to identify genomic rearrangements in individuals with apparently normal karyotypes [3]. Cryptic genomic rearrangements can lead to developmental disorders, although they can also occur as benign polymorphisms [4]. To date, CGH analysis and SNP genotyping have been carried out for patients with 46,XY DSD, identifying multiple submicroscopic deletions and duplications [5], [6], [7]. Such rearrangements frequently affected coding exons or regulatory regions of known DSD-associated genes including *SF1*, *SOX9* and *DMRT1*, or exons of candidate genes including *KANK1* and *ZEB2* [5], [6], [7]. These data suggest that genomic abnormalities at various chromosomal loci may underlie 46,XY DSD.

To clarify the role of cryptic genomic rearrangements in the development of 46,XY DSD, we performed copy-number analyses

for 24 patients. The results provide novel insights into the molecular basis of 46,XY DSD.

Subjects and Methods

Ethics Statement

This study was approved by the Institutional Review Board Committee at the National Center for Child Health and Development. After obtaining written informed consent from the parents, peripheral blood samples were collected from the patients. When possible, blood samples were also obtained from the parents.

Patients

The study population comprised 24 patients with 46, XY DSD, including nine cases with complete female-type external genitalia, five with ambiguous genitalia and 10 with male-type external genitalia with hypospadias (Table 1). None of the 24 patients had a family history of DSD or a history of prenatal exposure to specific environmental pollutants. G-banding analysis showed a normal 46,XY karyotype in all patients. Mutations in the coding regions of known DSD-causative genes, *SRY, AR, SRD5A2, SF1, WNT4, SOX9, WT1, BNC2, DMRT1, HSD17B3,* and *MAP3K1,* were excluded by sequence analyses.

CGH Analysis

Genomic DNA samples were subjected to CGH analyses using a catalog human array (4×180 k format, Agilent Technologies, Palo Alto, CA), according the manufacturer's instructions. The sizes and positions of the genomic rearrangements were analyzed using the UCSC genome browser (http://genome.ucsc.edu/; February 2009, hg19, build 37). In the present study, we focused on copy-number alterations with a physical size of more than 1.5 Mb, which have a higher probability of being associated with disease phenotypes [8]. Deletions and duplications registered in the database of genomic variants (http://projects.tcag.ca/variation/) were excluded as benign polymorphisms.

Results

CGH Analysis

We identified heterozygous submicroscopic deletions in three cases (cases 1–3; Fig. 1). The deletions affected several genes (Table 2). Case 1 harbored a ~8.5 Mb terminal deletion at 9p24.1–24.3 that encompassed *DMRT1,* in addition to 39 other genes. Case 2 carried a ~2.0 Mb interstitial deletion at 20p13 that included 36 genes. Case 3 had a ~18.0 Mb interstitial deletion at 2q31.1–32.1 that affected the entire *HOXD* cluster (*HOXD 1–13*), and 84 other genes. The parents of case 2 did not carry the deletion, whereas the parental samples of cases 1 and 3 were not available for genetic analyses.

Table 1. Patients analyzed in the present study.

Cases	Karyotype	Ethnic origin	External genitalia	Additional clinical features
1	46,XY	Japanese	Female	Mental retardation, schizophrenia
2	46,XY	Vietnamese	Ambiguous	Short stature
3	46,XY	Vietnamese	Ambiguous	Short stature, mental retardation, multiple anomalies
4	46,XY	Japanese	Female	
5	46,XY	Japanese	Female	Upper limb anomalies
6	46,XY	Japanese	Female	
7	46,XY	Japanese	Female	Short stature
8	46,XY	Japanese	Female	
9	46,XY	Japanese	Female	
10	46,XY	Japanese	Female	
11	46,XY	Japanese	Female	Agenesis of the corpus callosum, short palpebral fissures
12	46,XY	Japanese	Ambiguous	
13	46,XY	Japanese	Ambiguous	
14	46,XY	Indian	Ambiguous	
15	46,XY	Japanese	Male with HS	
16	46,XY	Japanese	Male with HS	
17	46,XY	Japanese	Male with HS	
18	46,XY	Japanese	Male with HS	
19	46,XY	Japanese	Male with HS	
20	46,XY	Japanese	Male with HS	
21	46,XY	Japanese	Male with HS	
22	46,XY	Japanese	Male with HS	
23	46,XY	Japanese	Male with HS	
24	46,XY	Vietnamese	Male with HS	

DSD, disorders of sex development; HS, hypospadias.
doi:10.1371/journal.pone.0068194.t001

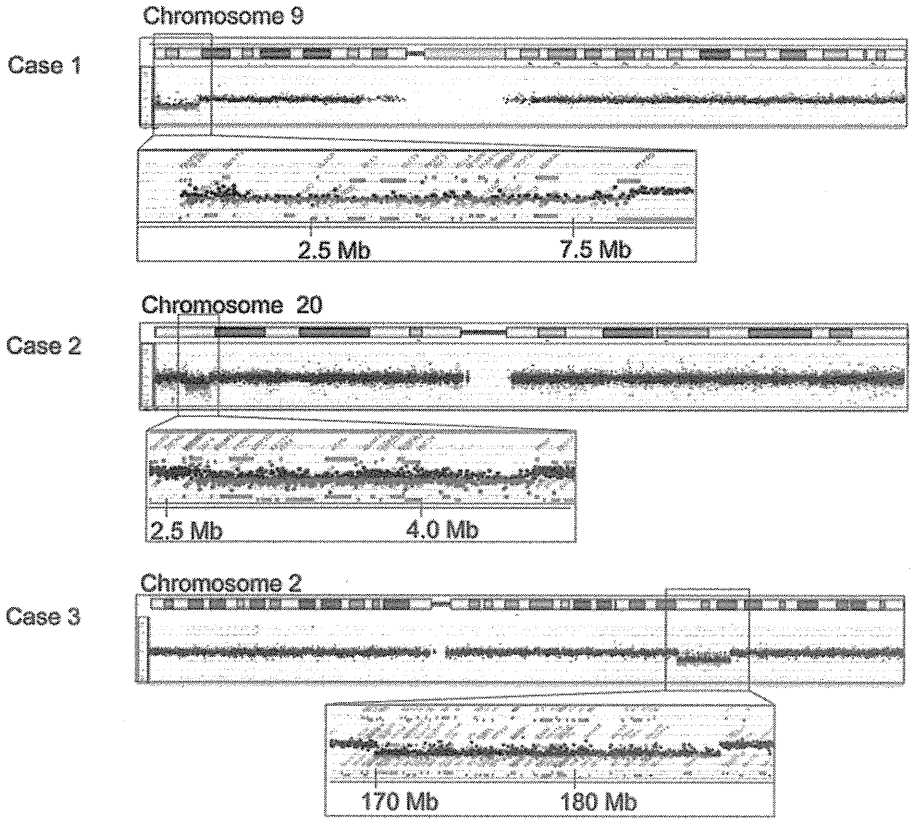

Figure 1. Cryptic heterozygous deletions in cases 1–3. CGH analysis identified heterozygous deletions in cases 1–3. The black, red, and green dots denote signals indicative of the normal, the increased (> +0.5) and the decreased (< − 1.0) copy-numbers, respectively. Genomic positions correspond to the human genome reference assembly (UCSC Genome Browser, February 2009, hg19, build 37). The names of the genes affected by the deletions are shown in Table 2.
doi:10.1371/journal.pone.0068194.g001

Clinical Features of Deletion-positive Patients

Case 1 was a genetic male born to non-consanguineous Japanese parents. This patient had complete female-type external genitalia and was raised as a female. This patient exhibited mental retardation and behavioral problems and was diagnosed as having schizophrenia. At 17 years of age, this patient was referred to our clinic because of primary amenorrhea. Clinical analysis detected no dysmorphic facial features or cardiac/renal abnormalities. Abdominal ultrasonography delineated a uterus. Blood endocrine tests indicated primary hypogonadism (Table 3). At 17 years of age, the patient underwent gonadectomy. Histological analyses showed bilateral streak gonads with ovarian ducts. The parents were clinically normal.

Case 2 was a genetic male born to non-consanguineous Vietnamese parents. At birth, this patient exhibited a micropenis, cryptorchidism, and distal hypospadias. Abdominal ultrasonography detected bilateral testes (12×6 mm) in inguinal canals. The uterus and ovaries were absent. This patient was raised as a boy and underwent surgical intervention for hypospadias and cryptorchidism at 4 years and 2 months and at 4 years and 3 months of age, respectively. On his visit at 4.5 years of age, the patient showed a penis with a stretched length of 3 cm, and left testis (12×9 mm) in the scrotum and right testis (13×6 mm) in the inguinal canal (Fig. 2). He had no dysmorphic facial features (Fig. 2). He showed short stature (89 cm, −2.9 SD) and delayed bone age (equivalent to 2 years of age). His mental development was normal. Blood endocrine tests at 4.5 years of age showed low levels of lutcinizing hormone and testosterone (Table 3). His growth hormone levels were within the normal range at the baseline, but remained low after physical exercise. His parents were clinically normal and had normal statures.

Case 3 was born to non-consanguineous Vietnamese parents at 40 weeks of gestation with a birth weight of 2.0 kg (−3.7 SD). At birth, this patient manifested severe micropenis and hypospadias (Fig. 2). Bilateral testes were palpable in the scrotum, and uterus and ovaries were absent. Thus, this patient was raised as a boy. In addition to genital abnormalities, he exhibited multiple anomalies of the fingers and toes, i.e., camptodactyly and flexion contracture of the proximal interphalangeal joint of the right index and left ring fingers, cutaneous syndactyly of the 2nd and 3rd toes and medial deviation of the 4th toe in the right foot, lateral deviation of the 2nd toe and medial deviation the 4th toe in the left foot, and overriding of the 4th toe on the third toe in both feet (Fig. 2). Furthermore, he showed dysmorphic facial features such as ptosis and micrognathia (Fig. 2). His blood testosterone level at birth was within the normal range (Table 3). On examination at 11 months of age, he showed obvious growth retardation (body weight; 6.0 kg, <−3.0 SD) and developmental delay (DQ <30). At one year of age, he presented with an episode of febrile convulsion. Brain magnetic resonance imaging detected delayed myelination, hypogenesis of the corpus callosum, and prominent ventricular and CSF spaces (Fig. 2). His parents were clinically normal.

Table 2. Genes affected by the cryptic deletions.

Case 1	Case 2	Case 3	
C9orf66	EBF4	BBS5	CHN1
DOCK8	CPXM1	KBTBD10	ATF2
KANK1	C20orf141	FASTKD1	ATP5G3
DMRT1	FAM113A	PPIG	KIAA1715
DMRT3	TMEM239	CCDC173	EVX2
DMRT2	VPS16	SSB	HOXD1-13
SMARCA2	PTPRA	C2orf77	MTX2
FLJ35024	GNRH2	PHOSPHO2	LOC375295
VLDLR	MRPS26	KLHL23	HNRNPA3
KCNV2	OXT	METTL5	LOC100506866
KIAA0020	AVP	UBR3	NFE2L2
RFX3	LOC100134015	MYO3B	NR_026966
GLIS3	UBOX5	LOC440925	AGPS
C9orf68	FASTKD5	LOC285141	TTC30B
SLC1A1	SLC4A11	SP5	TTC30A
SPATA6L	C20orf194	NR_046248	PDE11A
AK3	DDRGK1	GAD1	SNORD77
CDC37L1	ITPA	GORASP2	OSBPL6
RCL1	SLC4A11	TLK1	DFNB59
C9orf46	C20orf194	METTL8	FKBP7
JAK2	ATRN	DCAF17	PLEKHA3
INSL6	GFRA4	CYBRD1	LOC100506866
INSL4	ADAM33	DYNC1I2	TTN
RLN2	SIGLEC1	SLC25A12	CCDC141
RLN1	HSPA12B	HAT1	SESTD1
C9orf46	C20orf27	METAP1D	ZNF385B
CD274	CDC25B	DLX1	CWC22
PDCD1LG2	C20orf29	DLX2	UBE2E3
KIAA1432	SPEF1	ITGA6	ITGA4
ERMP1	CENPB	PDK1	CERKL
MLANA	MAVS	RAPGEF4-AS1	NEUROD1
KIAA2026	PANK2	RAPGEF4	SSFA2
RANBP6	RNF24	ZAK	PPP1R1C
IL33	SMOX	MLK7-AS1	PDE1A
TPD52L3	LOC728228	CDCA7	DNAJC10
UHRF2	ADRA1D	SP3	FRZB
GLDC		OLA1	NCKAP1
KDM4C		LOC285084	PDE1A
C9orf123		CIR1	DUSP19
PTPRD		SCRN3	NUP35
		GPR155	ZNF804A
		WIPF1	FSIP2
		CHRNA1	

doi:10.1371/journal.pone.0068194.t002

Discussion

We identified cryptic heterozygous deletions with physical sizes of more than 1.5 Mb in three of the 24 patients with 46,XY DSD. The results support the notion that submicroscopic genomic rearrangements constitute a portion of causative mechanisms for 46,XY DSD [5], [6], [7]. Furthermore, molecular and clinical data of the three cases imply that cryptic deletions can cause DSD as components of contiguous gene deletion syndromes. Since array-based CGH analysis and SNP genotyping can detect copy-number alterations across the entire genome in a single assay,

Table 3. Clinical and laboratory findings of cases 1–3.

Cases	Case 1	Case 2	Case 3
Molecular analyses			
Karyotype (G-banding)	46,XY	46,XY	46,XY
Genomic rearrangement	Deletion	Deletion	Deletion
Genomic position of the deletion	9p24.1–24.3	20p13	2q31–32
Size of the deletion	~8.5 Mb	~2.0 Mb	~18.0 Mb
Parental origin of the deletion	Unknown	*de novo*	Unknown
Clinical features			
External genitalia	Female-type genitalia	Ambiguous	Ambiguous
Mental retardation	Yes	No	Yes
Growth failure/Short stature	No	Yes	Yes
Dysmorphic facial appearance	No	No	Yes
Additional features	Schizophrenia	Delayed bone age	Skeletal anomalies
			Brain anomalies
			Convulsion
Endocrine data[a]			
Age at examination	17 y	4.5 y	at birth
LH (mIU/mL)	*17.4* (0.2–2.2)	**0.01** (0.2–1.9)	
FSH (mIU/mL)	*101.1* (0.6–4.8)		
Testosterone (nmol/L)	**0.71** (9–32)	**0.01** (0.2–0.5)	4.9 (<12)
GH after physical exercise (ng/mL)		**1.5** (3.0–28.3)	

DSD, disorders of sex development; MP, micropenis; HS, hypospadias; CO, cryptorchidism.
The hormone values below the reference range are boldfaced, and those above the reference range are italicized.
[a]Reference values of the age-matched control individuals are shown in the parenthesis.
doi:10.1371/journal.pone.0068194.t003

these methods should be considered for patients with 46,XY DSD, particularly for those with additional clinical manifestations.

Case 1 had a ~8.5 Mb heterozygous deletion at 9p involving 40 genes. Of the 40 genes, *DMRT1* is known to encode a male specific transcriptional regulator with a conserved zinc finger-like DNA-binding domain [9], [10]. Since mouse *Dmrt1* has been implicated in testicular differentiation [11], and intragenic deletions of human *DMRT1* have been identified in 46, XY patients with gonadal dysgenesis [6], [12], it appears that DSD in case 1 results from haploinsufficiency of *DMRT1*. These data argue for the assumption that heterozygous deletions involving the coding exons and/or the upstream region of *DMRT1* account for a substantial part of the etiology of complete and partial gonadal dysgenesis in individuals with 46, XY karyotype [6], [12], [13], [14]. Furthermore, our results provide additional information about other disease-associated loci. First, deletions at 9p22.3–23 are known to cause various malformations, such as craniofacial abnormalities, cardiac defects, and dysplastic kidneys, which are collectively referred to as the 9p- syndrome [13]. Lack of clinical manifestations of the 9p- syndrome in case 1 implies that the gene(s) responsible for this syndrome is not located in the ~8.5 Mb terminal region. This is consistent with previous studies which mapped the critical region of this syndrome to a genomic interval approximately 11–15 Mb from the telomere (Fig. 3A) [13]. Second, terminal deletions at 9p have previously been associated with mental retardation [13]. Our data suggest that a gene involved in brain development resides in the ~8.5 Mb terminal region that is deleted in case 1 (Fig. 3A).

Case 2 had a *de novo* ~2.0 Mb interstitial deletion at 20p13, which has not been identified previously in patients with DSD. Furthermore, none of the 36 genes affected by the deletion have been associated with sex development. These results, in conjunction with previous reports of hypomasculinized external genitalia in a patient with a ≥6 Mb deletion at 20p13-12.3 [15] and in a patient with a 20p11.2-pter deletion [16], indicate that the genomic interval spanning ~2.7–4.7 Mb from the telomere (deleted in case 2 and in the two aforementioned patients) encompasses a novel causative gene for DSD (Fig. 3B). However, the penetrance of DSD in males with 20p13 deletions appears to be low, because genital abnormalities have been described only in a small percentage of patients with such deletions [16], [17], [18], [19]. It might also be possible that the 20p13 and/or the 2q31.1–32 deletion has unmasked a recessive mutation of the testis development gene(s) on the structurally normal homologous chromosome, leading to DSD. In addition, the deletion of case 2 seems to harbor a gene that is indispensable for growth, because short stature was observed in case 2, as well as in most patients with partial monosomy of 20p [16], [17], [18], [19]. In this regard, although case 2 showed impaired growth hormone secretion after exercise, it remains to be clarified whether short stature in patients with 20p deletions is ascribed to growth hormone deficiency. Furthermore, unlike patients with terminal deletions of 20p [16], [17], [18], [19] case 2 showed no facial dysmorphism or mental retardation. These data indicate that a gene(s) involved in the development of the craniofacial region and brain resides within the 0–2.7 Mb interval from the telomere that is preserved in case 2. Consistent with this, facial abnormalities and developmental delay have been reported in two patients harboring 20p terminal deletions of less than 1.7 Mb [20] (Fig. 3B). Importantly, the deletion in case 2 includes *OXT* and *AVP* that are predicted to play